Optimization of Water and Nitrate Use Efficiencies for Almonds under Micro-Irrigation

Project No.: **13-PREC4-Hopmans**

Project Leader: Jan W. Hopmans
Department of Land, and, Air and Water Resources
UC Davis
One Shields Ave.
Davis, CA 95616
530.752.3060
jwhopmans@ucdavis.edu

Project Cooperators and Personnel:
Maziar M. Kandelous, Department of LAWR, UC Davis
Patrick Brown, Department of Plant Science, UC Davis
Blake Sanden, UCCE – Kern County

Objectives:

This field study provides critical information on the movement of water and nutrients through the soil under variable soil moisture conditions, and provides insight into the interactions of applied irrigation water and nitrogen fertilizer, soil physical properties, soil layering and crop root growth with nutrient use efficiency, minimizing losses of water (leaching and evaporation) and nitrogen (leaching and denitrification).

The final goal of this research project is to field-validate, optimize and refine the HYDRUS model under a variety of fertigation regimes using the on-going nutrient study in almonds implemented by P. Brown et al. Results will be used to optimize the management of irrigation and fertigation in an almond orchard. The specific objectives of this project are:

1. To determine optimal irrigation and fertigation practices for micro-irrigation (drip and micro-sprinkler) systems for almond, to improve water and nutrient use efficiencies, and to reduce leaching and gaseous losses of nitrates, using a wide range of possible management scenarios (water, fertigation, salinity);

2. To evaluate the results using the HYDRUS model from extensive field data for specific treatments, and refine it if so needed.

The objectives are achieved by collecting relevant field data such as soil hydraulic and textural properties with soil layering, monitoring of soil moisture and soil water potential, soil temperature and nitrate solution concentration for selected treatments, in addition to data already being collected as part of the larger nutrient management project. The data collection and analysis is very important, since all future model calibration and validation will be based on these data. A final optimization model will provide best management practices for various relevant micro-irrigation layouts with corresponding optimum irrigation and fertigation scheduling for a range of soil types.

Interpretive Summary:

Micro-irrigation methods have proven to be highly effective in achieving the desired crop yields, but there is increasing evidence suggesting the need for the optimization of irrigation scheduling and management, thereby achieving sustainable agricultural practices, while minimizing losses of applied water and nutrients at the field scale.

To optimize irrigation/fertigation of almonds, it is essential that irrigation and fertilizers are applied at the optimal concentration, place, and time to ensure maximum root uptake. Moreover, sound and sustainable irrigation systems must maintain a long-term salt balance that minimizes both salinity impacts on crop production and salt leaching to the groundwater. The applied irrigation water and dissolved fertilizer, as well as root growth and associated nutrient and water uptake, interact with soil properties and fertilizer source(s) in a complex manner that cannot easily be resolved with 'experience' and field experimentation alone. It is therefore that state-of-the-art modeling is required with the field observations, to allow for unraveling of the most obvious complexities as a result of the typical wide spatial variations of soil texture and layering across farmer-managed fields.

The goal of this research project is to optimize management practices for various micro-irrigation systems for almond, minimizing losses of water (leaching and evaporation), nitrogen (leaching and denitrification), and crop yields by water and salinity stress (droughts). In addition, the applied HYDRUS model with associated root water and nutrient uptake will be evaluated using extensive datasets as acquired from an ongoing nutrient management field project. Therefore, the research project consists of two main components: (a) determining the optimal irrigation and fertigation practices for micro-irrigation (drip and micro-sprinkler) systems for almond, to improve water and nutrient use efficiencies, and to reduce leaching and gaseous losses of fertilizer Nitrogen, using a wide range of possible management scenarios (water, fertigation, salinity), and (b) evaluation of the results using the HYDRUS model from extensive field data for specific treatments, and to refine it if needed.

To achieve this goal, this project emphasizes the collection of relevant field data such as soil hydraulic properties, soil texture, and soil layering, and continued monitoring of soil moisture, soil water potential, temperature, salinity, and soil solution nitrate concentration for selected irrigation type treatments. For each of the two irrigation treatments, soil profiles were analyzed to identify soil layers with corresponding textural and hydraulic properties. An extensive set of ECHO-TE soil moisture sensors (Decagon, Inc.), tensiometers, and soil water solution samplers were installed in the tree root zone to monitor the spatial and temporal changes of soil water content, total soil water potential, soil salinity, temperature, and soil solution nitrate. A special tensiometer was designed to monitor and estimate leaching rates of applied irrigation water and nitrate fertilizers.

The 2013-14 annual report focuses on the analysis of variation on applied water, soil water storage, and heterogeneity in soil textural and hydraulic properties at both tree plot and field scales. The ultimate goal of this analysis is to assess and evaluate leaching rates of water and nitrate fertilizer throughout the year for both irrigation treatments. In general, much of leaching amounts and rates are largely controlled by irrigation type, soil layering, and applied water (irrigation and precipitation) relative to evapotranspiration (ET). The combined installation of

tensiometers with solution samplers below the rooting zone are the best way to measure leaching rate of both water and nitrate. Although their operating range is limited to relatively wet soils, this is not a limitation for our purpose as leaching is only relevant if the soil is wet. The main limitation is caused by the large uncertainty of the soil's unsaturated hydraulic conductivity. We recommend using existing databases such as Neuro Multistep as applied in this study, and/or to using in-situ soil moisture and soil matric potential data to infer soil hydraulic properties by inverse modeling. It is shown that the deep soil profile in this study is fairly dry toward the maximum tensiometer range, suggesting negligible leaching of water and consequently nitrate under common irrigation/fertigation management practices of the past three years. Alternatively, we propose to apply a tree-scale and field-scale water balance technique using spatially-distributed soil moisture measurements to infer leaching rate and its spatial variations as caused by soil heterogeneity, and variation in applied water. We show that the water balance approach may lead to considerable leaching uncertainty unless all the components of the water balance equation are available at the same scale and their associate uncertainties are low. Tentatively, our data suggest that water and nitrate losses in our study area are low, because of the 3-year drought as caused by associated low winter/spring precipitation.

This past year, we focused on the water balance calculations from field-measured soil moisture and water potential data, to better understand the relation between local tree-scale and field-scale measurements. In the next year, we plan to focus on water balance simulations using HYDRUS, and to conduct a sensitivity analysis procedure that allows extrapolation of specific field outcome to other soil types.

Materials and Methods:

The presented methods were used for an almond orchard consist of two micro-irrigation systems, drip and fanjet. A total of 40 trees across the field were monitored in which 20 trees were located in drip block, and 20 trees in fanjet block. For each irrigation system (block), one tree was selected for detailed instrumentation for the purpose of real-time monitoring of soil-water and tree status. The study is part of an ongoing project at Paramount Farms in Lost Hills (near Bakersfield). A schematic of the location of monitored trees in the field, fanjet and drip block, and two heavily instrumented trees is presented in **Figure 1**.

Soil characterization

Among the most important information is an evaluation of the presence of soil layers, and the textural/hydraulic properties of each individual layer for typical soil profiles. Using the layering information obtained from soil cores in 2011, we took six undisturbed soil samples (8-cm diameter and 6-cm tall) around each of the heavily instrumented trees (one in fanjet, one in drip) to measure the hydraulic properties of deep soil profile (two depths of 190, and 210 cm each with three replicates) . The constant head method along with pressure cell (Tempe Cell) experiment was used to measure the soil water retention curves, saturated hydraulic conductivity, and unsaturated hydraulic conductivity functions for each layer. The soil hydraulic properties are required to (1) estimate soil water storage and retention, and (2) compute leaching rate from the unsaturated hydraulic conductivity using Darcy's equation (Eq. [1]). Also, the bulk density, porosity, saturated water content, and the soil texture of each individual core was determined. As it became clear early on that variability of soil texture and

layering was large, we collected a total of 160 additional soil samples to a soil depth of 2.5 m at both tree scale treatments. From these, the majority of soil samples (110 samples) were undisturbed samples (both using manual core sampler and hydraulic giddings), from which either soil bulk density and/or saturated hydraulic conductivity were measured. Rather than measuring the unsaturated hydraulic properties for each soil sample (which is time consuming and complicated), we used the neural network approach by Budiman et al. (2004). Based on past soil hydraulic measurements from SJV soils, this so-called Neuro Multistep method allows for prediction of soil hydraulic properties using more easily to obtain soil properties of soil texture, soil bulk density and saturated hydraulic conductivity. These soil samples, however, were taken to evaluate the variability of soil physical and hydraulic properties and layering at tree scale. Therefore, to evaluate the field scale heterogeneity and variability in layering, a total of 360 additional undisturbed soil samples (one sample at each 30-cm depth interval down to 2.7 m, from each of the 40 monitored trees) were collected and analyzed to obtain the field mean and variation of bulk soil density, porosity, and soil texture.

Soil monitoring

Soil moisture and soil water potential

Unfortunately, many of ECHO-5TE (Decagon Inc) soil moisture sensors installed by PureSense in 2011 were useless, because of malfunctioning of sensors and data collection issues. Therefore, we installed a new set-up in 2012. A total of 30 ECHO-5TE (Decagon Inc.) soil moisture sensors were installed in the rooting zone of each of the two tree locations in a grid pattern (**Figure 2**), thereby instrumenting one quarter of the tree's rooting zone, at depths of 30, 60, 90, 120 and 150 cm for 6 spatial locations (**Figure 3**). An additional set of sensors were installed at the same depths below the berm in the fanjet plot along the center line (Y-direction) (**Figure 3**). The sensor installation grid was designed such that measurements provide soil information halfway between trees (Y direction), and up to the distance influenced by wetting pattern of either fanjet or drip perpendicular to the trees row (in X direction).

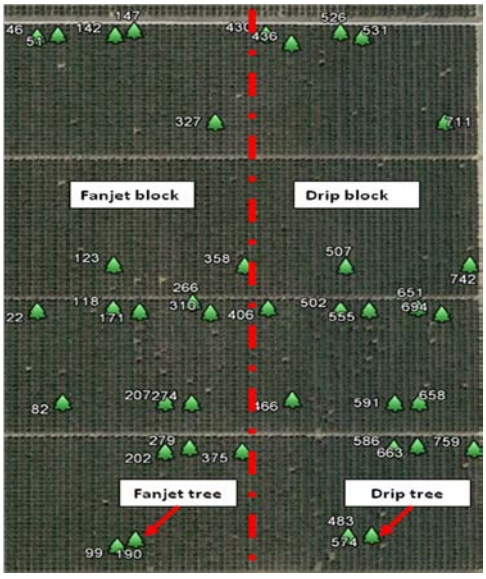

Figure 1. Locations of monitored trees in almond orchard (field), two irrigation systems (Fanjet and Drip block), and the two heavily instrumented trees (Fanjet and Drip tree).

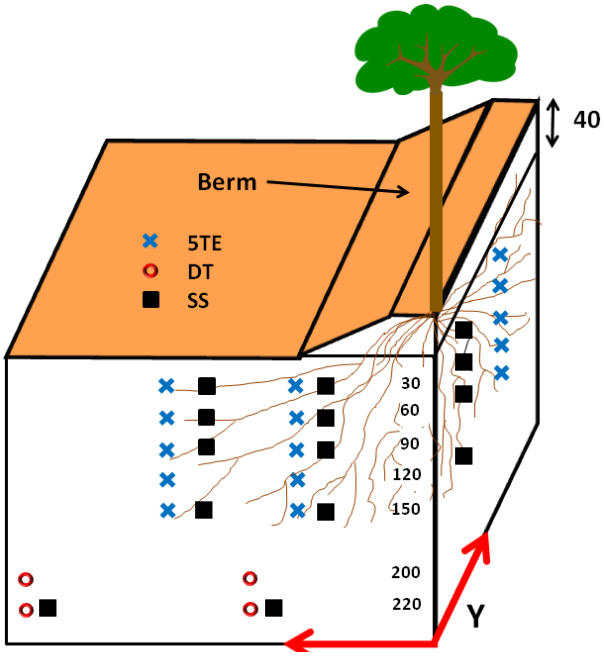

Figure 2. A schematic showing installation depths of various sensor types, with 5TE representing the ECHO-5TE soil moisture, DT the deep tensiometers, and SS is referring to soil solution samplers.

The ECHO-5TE provides for measurement of volumetric soil water content, as well as for soil salinity (Electrical Conductivity or EC), and soil temperature. For the purpose of installation, holes were dug with a 5" hand auger. Sensors were provided and are being monitored by PureSense Environmental Inc.

Four pairs of deep tensiometers (red circles) were installed at both fanjet and drip irrigation sites to monitor the total head gradient below the root zone. Two pairs of tensiometers were installed below the canopy where the irrigation water is applied representing the wet part below the root zone and the other two pairs were placed at the middle distance between two tree rows, representing the most dry region for both treatments.

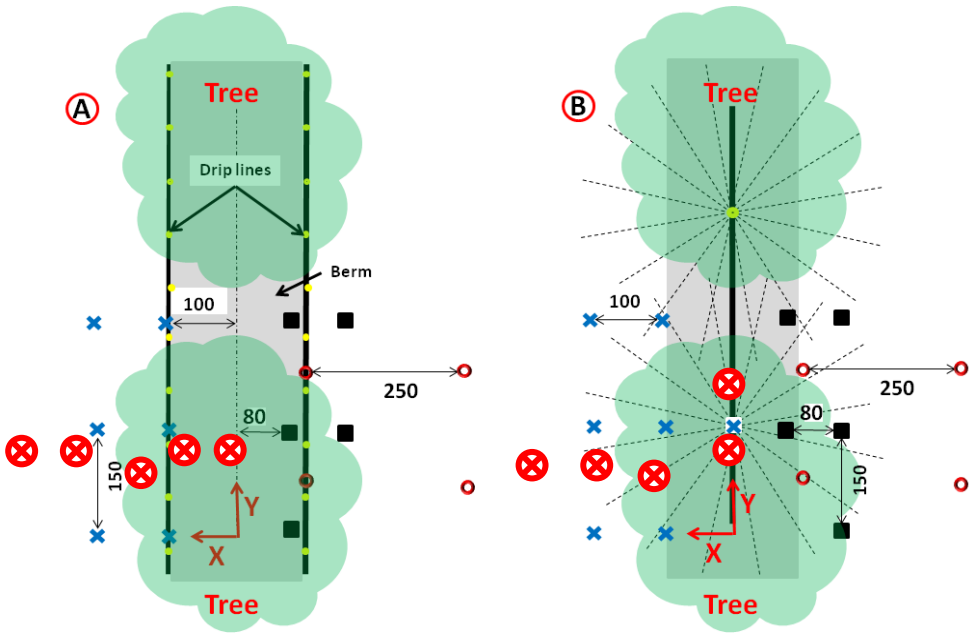

Figure 3. A schematic top view of the installed soil moisture sensors, deep tensiometers, and solution samplers in (A) Drip and (B) Fanjet site. The red crossed circles denote the approximate location for the neutron probe access tubes.

In addition, five neutron probe access tubes were installed in neighboring tree plots (**Figure 3**) for each treatment, allowing for soil moisture and soil water storage measurements to a depth of 2.7 m in 30-cm depth intervals. In addition to the two 5-probe instrumented (called hereafter heavily instrumented) trees, a total of 38 trees were instrumented with a single access tube in order to monitor the soil water storage at the field scale. The location of the single access tube relative to its nearby tree trunk was the same for each instrumented tree across the field, and corresponded to the location of the third access tube for the heavily instrumented trees. Most of the neutron probe measurements were collected approximately one day prior to each irrigation event. The neutron probe was calibrated using independent gravimetric soil moisture samples using linear regression, with a non-zero intercept (See **Figure 4A**). We note that the

soil water storage estimated using a single access tube is not as representative for the tree-scale as determined from instrumented trees using 5 neutron access tubes. Therefore, for each of the two heavily instrumented trees, the measured soil profile water storage using the 5-tube setup was correlated to the water storage using only the main access tube across the field (**Figures 4 B and C**), and this correlation was subsequently applied to single-access-tube monitored trees (**Figure 3**), for computation of the field-scale water balance.

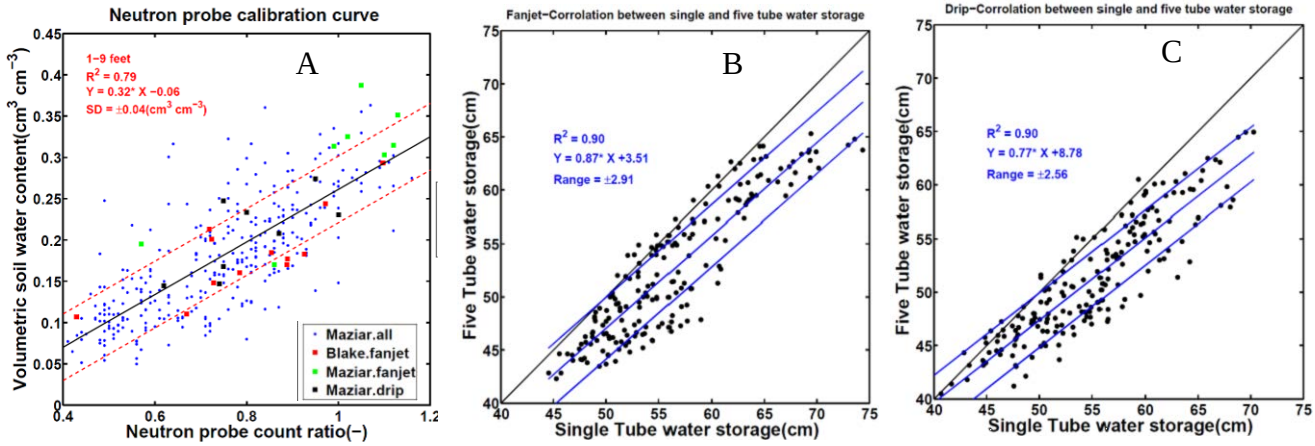

Figure 4. A: Neutron probe calibration curves with blue circles representing samples from entire orchard, green and black square remarking the data point from the heavily instrumented tree in fanjet and drip, respectively, and the red square showing additional data pointed collected by Blake Sanden from heavily instrumented tree in fanjet. **B:** Correlation between soil water storage using single probe and 5-probes setup in fanjet tree. **C:** Correlation between soil water storage using single probe and 5-probes setup in drip tree.

Leaching rate calculations

Leaching rates can be estimated if the hydraulic conductivity and the total head gradient across the soil layer below the root zone are known. The leaching flow rate, q_{AB}, can be calculated using the Darcy equation as follows:

$$q_{AB} = -K(h)\frac{H_B - H_A}{\Delta z_{A-B}} \; or \; q_{AB} = -K(\theta)\frac{H_B - H_A}{\Delta z_{A-B}} \quad , \qquad (1)$$

where *q* denotes the Darcy water flux (inches day $^{-1}$), *K(h) or K(θ)* represent the unsaturated soil hydraulic conductivity, which is a function of the soil matric potential *h or θ* at the deep measurement depth. In the Darcy equation, H_A and H_B denote the total water head values at bottom and top of the soil layer below the root zone, respectively, and Δz_{A-B} signifies the thickness of the soil layer between the tensiometers. As shown in **Figure 2** the set of deep tensiometers were installed at four different locations at depths of 200 and 220 cm. Using the measured soil matric potential values above and below the impeding layer and its thickness, we computed the total head gradient for each of four individual measurement locations for each site. Using the measured soil water matric potentials and soil water content along with the unsaturated hydraulic conductivity for the soil layer in question, one calculates the leaching rates by multiplying the unsaturated hydraulic conductivity with the total head gradient, according to Eq. [1]. The choice of using either water content or pressure head measurements for the conductivity estimation depends on the accuracy of the measurement and the

sensitivity of either of the two variables on the unsaturated hydraulic conductivity value (see soil textural analysis section). We used the hydraulic conductivity based on soil matric potential, K(h), as we concluded that the measured soil matric potential measurements with the deep tensiometers were very accurate in the wet soil moisture range.

Additional required input data for modeling

In addition to soil physical characterization, other required input data for the HYDRUS modeling includes measurements of tree evapotranspiration (ET), water application rates and spatial distribution for the drip and fanjet systems, fertigation amounts and rates, and tree root distribution. Daily ET rates are available from eddy-covariance data collected at the fanjet site, whereas volumetric flow rates are determined from flow meter measurements installed in the irrigation lines.

Figure 5. Measurement (a and b) of water application uniformity and uniformity pattern (c) for the fanjet (1 hour volume measurements).

The wetted area for the drip system is monitored by visual inspection, whereas the water application uniformity of the fanjet system was determined from measurement of water volumes in 110 10-cm diameter catch cans, distributed within the quarter section of the instrumented fan jet plot (**Figure 5**). Though additional uniformity data will be collected, soil moisture patterns indicate that the measured patterns are consistent during the irrigation season.

Water balance

In addition to estimation of leaching rates using the Darcy equation from tensiometric measurements (Eq. 1), leaching rates (L) can be determined from the tree-scale and field-scale water balance, using measurements of applied irrigation water (IW), precipitation (P), tree evapotranspiration (ET), and changes in soil water storage (ΔS) to a specific soil depth below the rooting zone. As the depth of the soil water storage measurements increase, we expect the estimated L to be more accurate, as it would increasingly account for upward capillary rise, if relevant. Thus, from periodic measurements of ΔS, and corresponding data of IW (flow meter measurements), P (CIMIS station #146), ET (eddy covariance tower) and ΔS (neutron probe), the leaching rate (L) can be computed from the following equation with the measurement unit expressed in depth of water (cm).

$$L = IW + P - ET - \Delta S \quad , (2)$$

The water balance was computed between irrigation events across the 2009-2013 monitoring season. Whereas IW, P, and ET are area-wide measurements, we divided the heavily instrumented tree plot in two equal size sections, representing the tree rooting zone (along the

tree rows) and dry zone (section between tree rows), where ΔS from the dry zone was determined from the neutron probe measurements furthest away from the tree row. The amount of water applied through irrigation system (IW) was monitored from flow meters for each site. The water volume delivered to each tree was divided to the area occupied by each tree yielding the equivalent depth of applied irrigation water. The number of dripper (20 drippers of 4 l/hr per tree) were designed such that the amount water delivered to each tree was equal to the amount of water applied to each tree of the fanjet site (2 fanjets of 40 l/hr per tree). Because of malfunctioning of soil water content sensors in 2013, it was decided to analyze the water balance for the 2009-2013 periods only, and to not further consider water content data after June, 2013.

Nitrate sampling

A total number of 20 shallow soil solution samplers were installed in both fanjet and drip irrigation systems (black square in **Figures 2 and 3**) to monitor the soil root zone nutrient status after each fertigation throughout the year. Additional four deep solution samplers were installed close to the deep tensiometers to measure the nitrate concentration of leached irrigation water (**Figure 3**). From the measured soil solution nitrate concentration the mass of leached nitrate can be computed by multiplying nitrate concentration with the soil leaching rate (L), as computed from **Eq. 1.** For that purpose, the solution nitrate concentration was multiplied by the depth-corresponding soil volumetric water content, thereby converting the mass of nitrate per volume of soil solution to the mass of nitrate per volume of soil.

Soil solution samples were taken every day starting from the day before until three to four days after each fertigation, by applying a 60-70 cbar vacuum to the solution sampler at the end of the day, with solution collected in the morning of the following day. The collected samples were kept cold (under ice) until analyzed in the lab for nitrate concentration measurement using a Shimadzu BioSpec-mini UV/Visible scanning spectrophotometer (540 nm). Having available periodic measurements of the applied fertilizer N and the amount stored in the tree's biomass (nuts and leaves), nitrate leaching rates could be computed from a nitrate mass balance. However, insufficient soil nitrate data were available for most of the monitoring period because of too dry soil conditions, making soil solution extraction impossible.

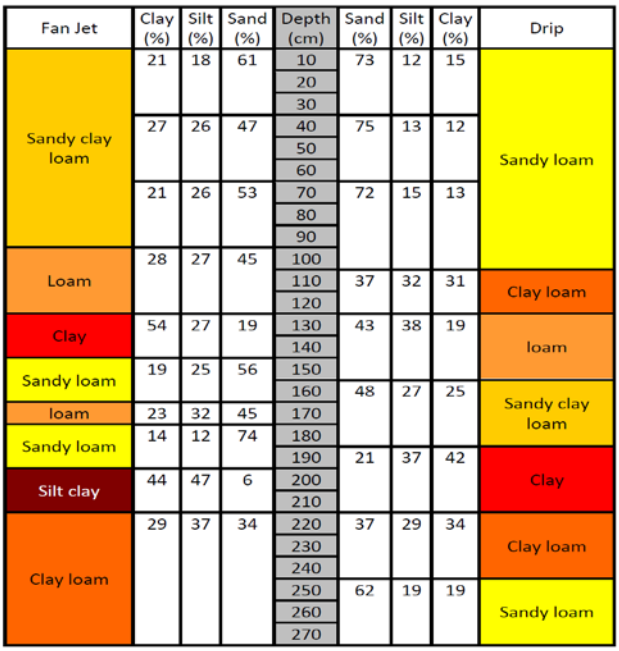

Figure 6. A schematic with soil layers and soil texture for the drip and fanjet sites.

Results and Discussion:

Soil textural analysis

Analysis of soil texture for both the fanjet and drip trees showed that the soil profile of the studied almond orchard is highly heterogeneous and layered. **Figure 6** shows representative soil layers and differences of soil profiles between the drip and fanjet tree. The top one meter

of soil profile at the fanjet site consists of coarse soil material, allowing quick infiltration of applied irrigation water. The profile includes two 20 cm thick fine-textured soil layers at approximate depths of 130 and 200 cm soil depth.

We believe the difference in depths of clay layers between the two irrigation plots has significant implications on leaching rates. These layers will prevent and/or delay downward water movement below the root zone. The drip site shows depth variations in soil texture as well, with the fine-textured soil layer at about the 180 cm.

Further soil core sampling at both experimental sites was needed to ascertain the depth variation of soil texture and hydraulic properties and their spatial heterogeneity of soil profiles within and between the two irrigation sites. **Figure 7** present the spatial heterogeneity of soil properties and layering within and between Drip and Fanjet irrigation sites in both tree (heavily instrumented trees) and field (single-access-tube equipped trees) scale. Although there are significant variations in soil layering and textural/hydraulic properties, the soil layering at tree scale plots follow the same pattern as was identified at the beginning of this project (**Figure 5**). Also, there is consistency in the data, with depth variations in saturated hydraulic conductivity (Ksat), coinciding with either depth variations in soil bulk density or sand/clay content. For example, the clay and clay loam layers in **Figure 6** correspond with soil layers of decreasing Ksat for both the drip (100 and around 200 cm) and fanjet (100 and 180 cm) sites. Despite the huge variation in soil layering and textural properties at the field scale, our interpretation is that the field scale layering and depth variation in bulk density in each irrigation site corresponds somewhat with that determined from the single tree soil profiles. Specifically, the sand content is maximum at depths near 30 and 180 cm across the field for the fanjet treatment. For the drip site, both the tree and field scale plot s show correspondence of coarse-textured soils in the top 100 cm soil profile.

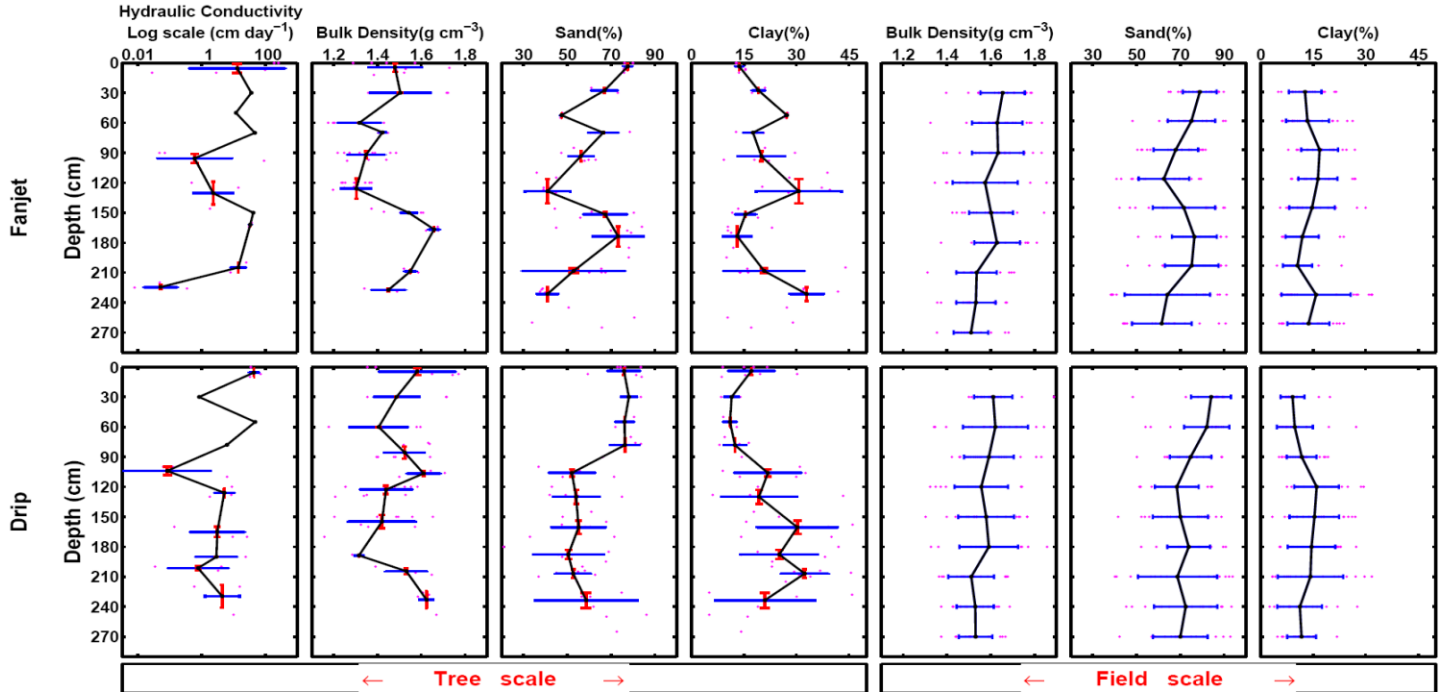

Figure 7. Mean (black line) and standard deviation (blue horizontal lines) values of saturated hydraulic conductivity (Ksat), dry bulk density, sand and clay content as a function of soil depth.

Soil hydraulic properties

Figure 8 shows the soil water retention and unsaturated hydraulic conductivity curves for the six core samples from the deep soil profile at depth of 190 and 210 cm. The soil water retention curve was measured using the Tempe cell method along with the constant head approach for saturated hydraulic conductivity. The results show the enormous variability of the soil water retention curves, thereby resulting in high uncertainty of the unsaturated hydraulic conductivity.

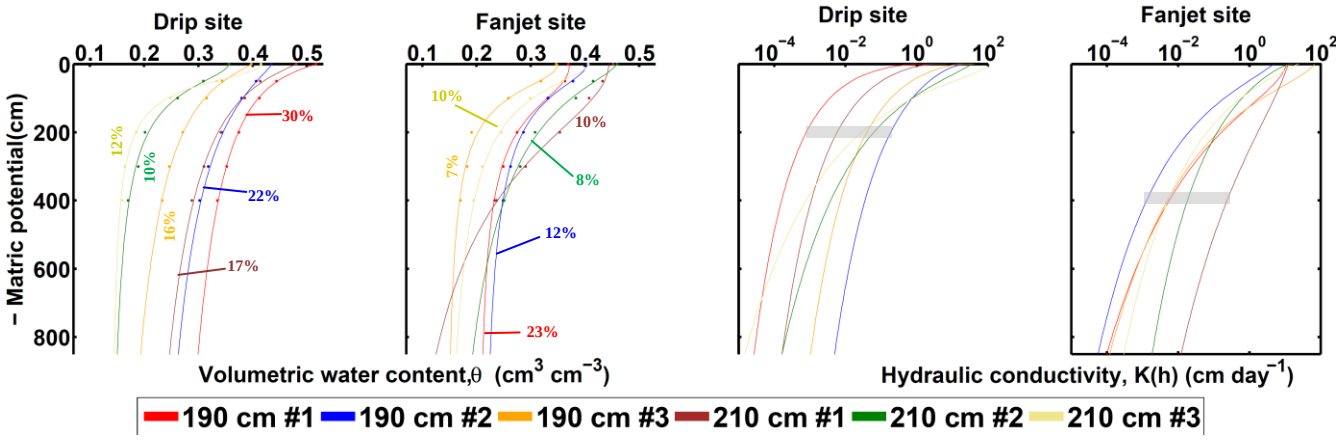

Figure 8. Soil water retention (left plots) and unsaturated hydraulic conductivity (right plots) curves for the different soil types and for drip and fanjet sites. The data points represent the measured data. The clay content values for each core are listed for each soil sample.

Though not shown in this report, we previously compared the Neuro Multistep predictions with measured hydraulic functions and concluded that the predicted curves agreed fairly well with the measured ones. Hence, it was decided to apply the Neuro Multistep model to predict both the soil water retention and unsaturated hydraulic conductivity curves using the soil physical data from the collected 21 soil samples (12 samples from drip and 9 samples from fanjet site) of the 200-240 cm depth interval for both tree plots. The results are presented in **Figure 9,** with the corresponding soil physical property values used for the prediction in **Table 1.** From the curves in **Figure 9**, it becomes instantly clear that the variation in soil water retention and unsaturated hydraulic conductivity is enormously large, even when considering the 200-240 cm depth interval only. Hence, accurate information of soil textural properties (both mean and variation) is extremely important to estimate leaching rates and its field-scale variations. Comparing the hydraulic conductivity curve as function of soil water content (θ, bottom panel) with the hydraulic conductivity curve as function of soil matric potential (h, center panel) one readily determines that a small uncertainty in soil water content results in a huge uncertainty in predicted unsaturated hydraulic conductivity. In contrast, when considering a similar range of uncertainty in the measured soil matric potential, the uncertainty of the predicted hydraulic conductivity is relatively small. Therefore, when estimating leaching rates (L) using Eq. [1], we will use the K(h) function in concert with soil water matric potential measurements.

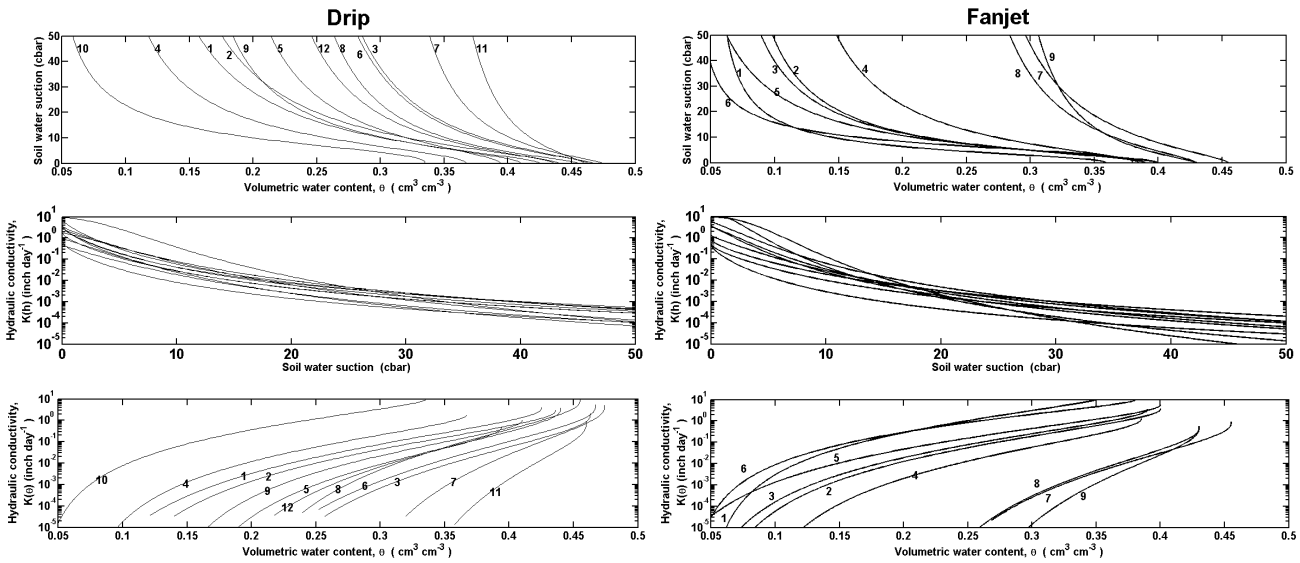

Figure 9. Soil water retention (top panel) and unsaturated hydraulic conductivity curves for the different soil samples taken for the 200-240 depth intervals for both the drip (left) and fanjet (right) sites. The center panel presents the predicted unsaturated hydraulic conductivity curves as function of soil matric potential; whereas the two bottom plots present the unsaturated hydraulic conductivity curves for the same soils, as function of soil water content.

Table 1. Soil variation in textural and physical properties for soil samples presented in **Figures 8** and **9** (200-240 soil depth, for 12 samples from drip and 9 samples from fanjet plot).

	Drip					Fanjet				
#	Sand (%)	Silt (%)	Clay (%)	Ksat (cm/day)	Bulk density (g/cm^3)	Sand (%)	Silt (%)	Clay (%)	Ksat (cm/day)	Bulk density (g/cm^3)
1	52	33	14		1.32	74	24	2	25.35	1.52
2	46	40	14		1.28	66	18	16		1.52
3	48	14	38	23.65	1.34	67	19	14	8.2	1.54
4	65	25	10	0.69	1.60	60	24	16		1.59
5	43	41	16	0.025	1.55	69	19	12	0.051	1.46
6	58	5	37	3.3	1.51	78	19	3	0.051	1.47
7	45	9	46		1.57	39	29	32	0.356	1.34
8	63	7	31		1.65	38	30	32		1.52
9	41	45	14	0.58	1.47	38	21	42		1.49
10	75	20	5		1.61					
11	12	42	46		1.64					
12	57	13	30	4.19	1.58					

Soil moisture measurements

To assess the accuracy and uncertainty of the EchoTE-5 soil moisture sensors, we took selected soil samples near the soil surface (depths of 30 and 60 cm) for a wide range of soil moisture conditions and both irrigation sites, and compared those with nearby (within 30 cm distance) sensor measurements. As is shown in **Figure 10**, the soil water content measured with the 5-TE sensors is within about 4 % (volumetric water content) of the independently measured soil water content, as determined from the 67% uncertainty band (red dotted lines). We realize that the accuracy is also controlled by spatial soil moisture variations within the sampled 30-cm separation distance, as determined by soil variability, sampling error and non - uniform water applications.

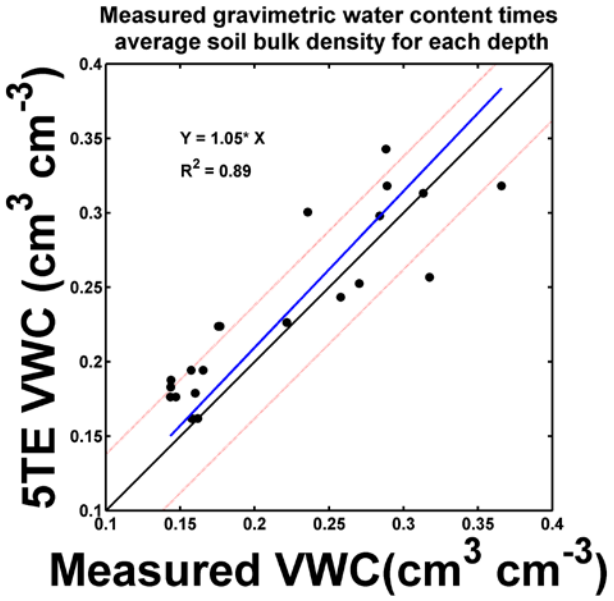

Figure 10. Calibration curve for ECH2O 5-TE water content sensor. Black circles represent the data points, whereas the dotted red lines show the 67% uncertainty band around the 1:1 black line. The blue line is the fitted line by linear regression (R2 = 0.89).

Figures 11 and 12 present the spatial and temporal variation of soil water content in the root zone for the drip and fanjet irrigation site for new installation setup, respectively, as obtained from the EchoTE-5 real time measurements, every half an hour, starting April 1, 2012. The pink and blue bars indicate the irrigation and rain events during the presented time period, respectively. The (X, Y) notation represents the Cartesian coordinate system, with both X and Y, representing distances (cm) from the tree trunk. For example, the panel with the (0,150) notation presents soil water content data that is exactly along the tree row (X = 0 cm) and midway between the trees (Y = 150 cm). Similar to the 2011 data set the sensors installed at depths of 30 and 60 (and 90 cm added at 2012) of the drip site (**Figure 11**) respond to the irrigation and precipitation events showing the affected soil profile by the moving wetting front. The mild response of Echo sensors at the 120 and 150 cm soil depth along with their relatively high and constant water content values is a reflection of the perching of water above the 180-220 cm depth clay layer (**Figures 6** and **7**). The spatial variation in soil water content at depths 120 and 150 cm confirm the soil heterogeneity presented in **Figure 7**, demonstrating variable-textured soil layers at the tree plot scale. Both the decreasing and constant water content at depths of 120 and 150 cm during the winter season suggest that precipitation amounts were relatively small or was largely intercepted by the tree canopy, since neither shallow sensors responded to those precipitation events. Comparing the minimum soil water content during the growing season and winter, we conclude that the soil water content remains at its lowest level during the winter, thus suggesting that the soil moisture profile was not affected by winter rainfall.

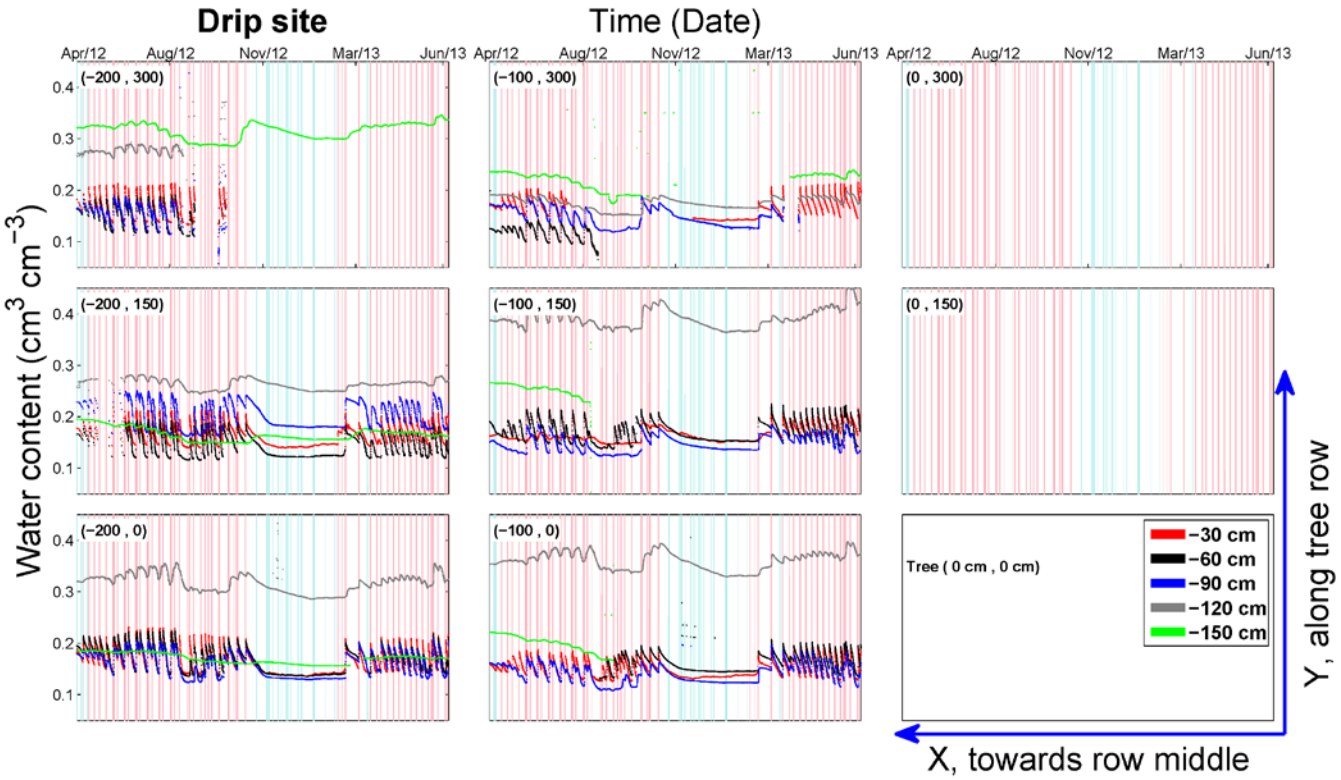

Figure 11. Spatial and temporal variations of soil water content in the root zone under **drip** irrigation system for 2012-13. The pink bars indicate irrigation events and the blue bars denote the precipitation events. The width of each bar represent the duration of each irrigation or precipitation events.

For the fanjet soil moisture measurements of **Figure 12**, the shallow sensors at depths of 30 and 60 cm immediately responded to irrigation events, but to a lesser extent than for the drip irrigation treatment, which is due to the larger application area for the fanjet as compared to the drip site. Comparing the temporal variations of water content at depths of 30 and 60 cm for locations (-100, 150) and (-200, 150) between the 2012 and 2013 irrigation seasons shows that the local soil moisture response was much larger, as caused by the installation of a single dripper along the water application line for the purpose of increasing water application rate without increasing irrigation duration. The clay layer at the 120 cm depth (**Figure 6**) is the main reason that there the water content is highest, as caused by the perching infiltrated soil water. Low water content values at the 150 cm soil depth can be explained by reduced leaching across the clay layer, with spatial variations caused by the non-uniform water application pattern and soil heterogeneities. In fact, spatial variations in root zone water content can be related to either the water application pattern of **Figure 5** or the soil heterogeneities presented in **Figure 7**.

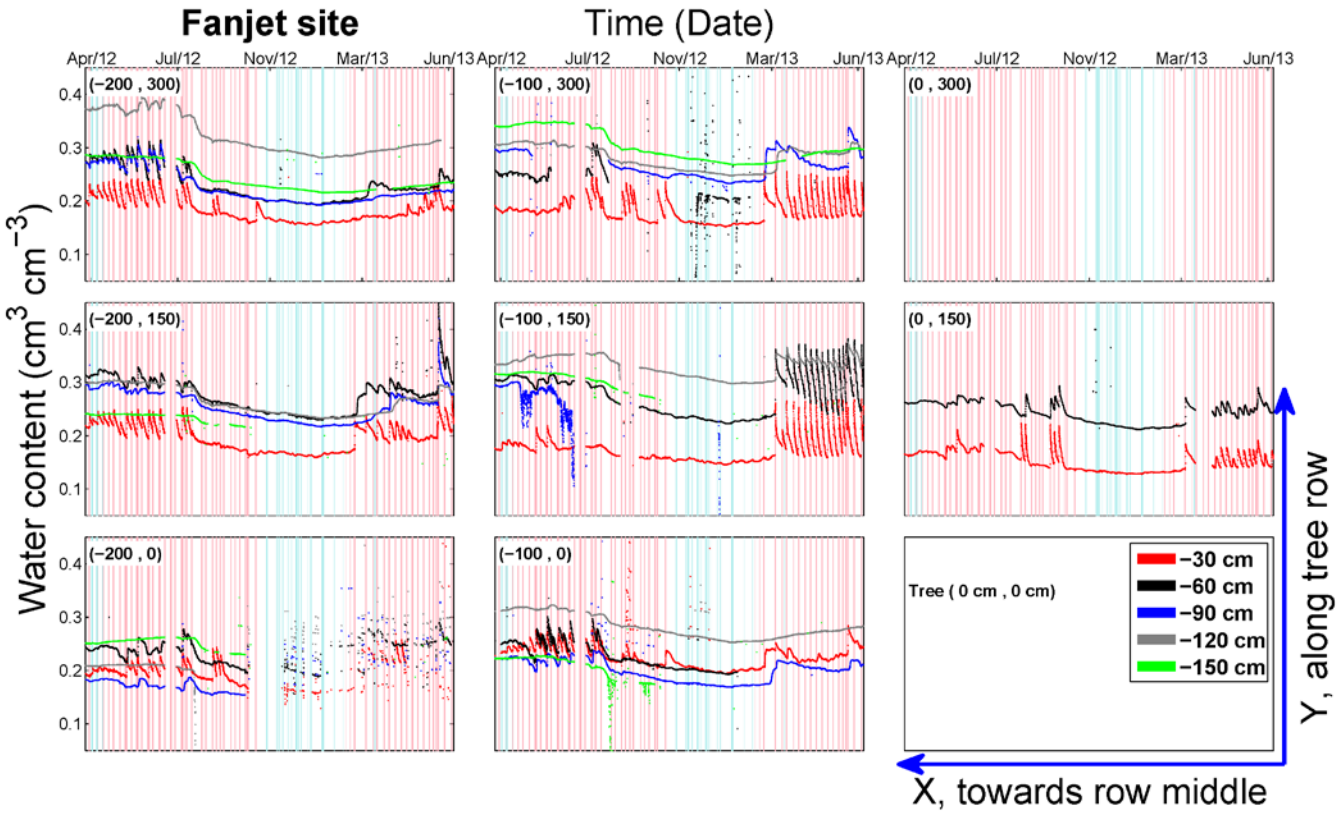

Figure 12. Spatial and temporal variations of soil water content in the root zone under **fanjet** irrigation system for 2012-13. The pink bars indicate irrigation events and the blue bars denote the precipitation events. The width of each bar represent the duration of each irrigation or precipitation events.

Leaching rate

The amount of water leaching (L, cm) for both irrigation sites was analyzed using two different approaches. The first method uses the water balance at two scales of tree plot and field, from measurements of applied water, evapotranspiration, and soil water storage measurements (section water balance). In the second approach, we applied Darcy equation [1], to compute leaching rates from tensiometric soil water potential measurements, and measured soil hydraulic properties along with predicted unsaturated hydraulic conductivity values using the Neuro Multistep method (refer to Darcy equation section). The presented water balance was computed for the 2009 - 2013 period.

Water balance[1]

Precipitation (P) and Evapotranspiration (ET):

Figures 13 A and B-(Fi, Dr, and Fn) show the cumulative precipitation and evapotranspiration of the water balance equation, with **Fi**, **Dr**, and **Fn** denoting field, drip, and fanjet data. The precipitation data (**Figure 13 A**) come from a nearby CIMIS station (#146) and was assumed representative for the whole field (both drip and fanjet treatments), so that precipitation rates were the same for the water balance, irrespective of scale (field, irrigation block (Drip and Fanjet), or tree plot. The amount of precipitation in the first two years (late fall 2009 and 2010 and early winter 2010 and 2011) was significantly higher as compared with the last two years.

[1] *Collaboration with Blake Sanden, farm advisor in Kern County, UC Extension Center.*

Depending on the soil profile water storage during the rain season, the precipitation water may be stored in the soil profile or leave the rooting zone as deep percolation if the soil water content exceeds the field capacity. The second panels from the top (**Figure 13 B**) show the cumulative actual evapotranspiration (ET_a) obtained by Eddy-Covariance tower located in the orchard for four consequence years. Similar to the precipitation data, we assumed that ET rates were identical, irrespective of scale. Comparing the precipitation and evapotranspiration data, it is shown that the amount of precipitation is about 10% of evapotranspirative demand indicating the irrigation dependency of the agricultural practice in the studied area.

Applied irrigation water (IW) Field Scale:

Figures 13 C (Fi, Dr, and Fn) show the cumulative amount of water applied for four consecutive years of the 2009 – 2013 for field, drip site, and fanjet site, respectively. In contrast to the precipitation and evapotranspiration which was assumed to be uniform across the field, the amount of applied irrigation water was determined locally using 30 flowmeters[2] installed across the field (15 in drip site, and 15 in fanjet site). The origin of variation presented in **Figure 13 C** is from two sources of a) the uncertainty associated with flowmeter readings, and b) the variation in applied irrigation water between different locations across the orchard. Our data show that there is ±7 % variation in IW across the orchard which corresponds to 72 cm (29 inches for four years) difference between minimum and maximum applied water, indicating the non-uniformity associated within and between the two irrigation systems. **Figure 14** shows the location of flow meters installed across the field, in which the relative variation of IW is shown by circle size. **Figures 13** and **14** shows that the average and variation in applied water in drip site are higher than fanjet site, suggesting either greater change in soil water storage or higher leaching for the drip site. It may also result in higher ET in drip site, but there is no independent measurement of ET to evaluate the difference between ET in drip and fanjet. However, in a field scale evaluation it is shown that the sum of field averaged applied water and precipitation data is equal to the evapotranspiration measured by Eddy-Covariance tower confirming a well managed field with irrigation scheduling based on ET.

Tree Scale:

Figure 14 C (Dr and Fn) show the cumulative amount of water applied for four consecutive years of the 2009 – 2013 for two heavily instrumented trees in drip and fanjet sites, respectively. The location of these two trees are shown in **Figure 14** and marked as “5-NP” indicating the five neutron probe access tubes installed for each tree. The variation in applied water for both trees is assumed to be very small, as it was controlled by the flowmeter specifications. However, we realized that in reality this variation within the tree plot is larger, but could not be measured. There is a large difference between applied water in drip and fanjet tree, such that the IW in drip tree is 6.5% higher while in fanjet site it is 4.8% smaller than the field scale average applied water. Similar to the field/irrigation block scale and assuming a uniform ET throughout the orchard the drip tree was over irrigated, while the fanjet tree was under irrigated.

[2] *There were initially total of 30 trees with flowmeters starting from 2009, but 10 trees were added in 2010. Hence, we used the initially 30 monitored trees to cover four years of 2009-2013.*

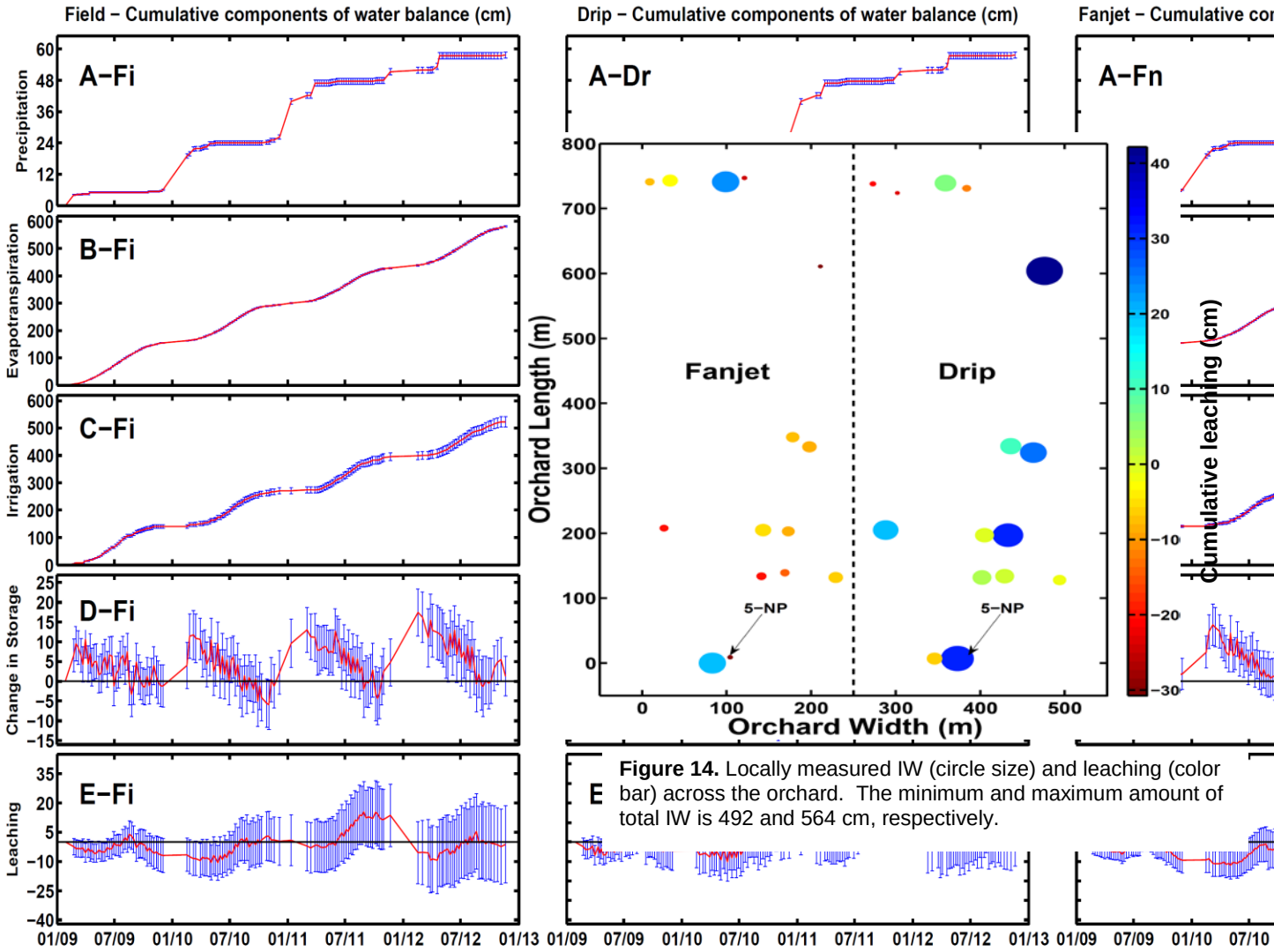

Figure 14. Locally measured IW (circle size) and leaching (color bar) across the orchard. The minimum and maximum amount of total IW is 492 and 564 cm, respectively.

Figure 13. Cumulative amount of (A) precipitation, (B) evapotranspiration, (C) applied irrigation water, (D) change in soil water storage, and (E) leaching in three scales of field (left), drip (middle) and fanjet (right) plot for four consecutive of years of 2009-2013. Average values are presented by the thick red lines, whereas the spatial variations are presented by the error bars, defined by standard deviations.

<u>Soil water storage (ΔS):</u>

The last component of the water balance equation that is required for leaching calculations is the change of soil water storage. We used the available neutron probe data, as these provided soil water content measurements down to 2.7 m.

<u>Field Scale:</u>

Figure 13 D (Fi, Dr, and Fn) show the cumulative changes in soil water storage for four consecutive years of the 2009 – 2013 for field, drip block, and fanjet block, respectively. The soil water storage increase by winter precipitation when the crop water demand is the lowest and it decreases during the growing season when soil water storage by ET or leaching. On an annual basis, it is shown that the soil water storage does not change. The uncertainty presented in these figures are considerably high and are originated from three sources of a)

the uncertainty in Neutron Probe calibration curve presented in **Figure 4 A**, **B**) the uncertainty in transformation curve from one- to five- access tubes (**Figure 4 B** and **C**) the variation between different locations across the orchard (**Figure 14**).

Tree Scale:

Figure 15 D (Dr and Fn) show the cumulative changes in soil water storage for four consecutive years of the 2009 – 2013 for drip, and fanjet tree, respectively. The presented soil water storage changes follow the same trend shown in the field scale, with increasing soil water storage by precipitation and irrigation in the winter and spring followed by depletion cycles throughout the growing season. The overall soil water storage in Fanjet tree increase from one year to another and this is because of the initially dryer soil water profile at fanjet tree at the beginning of this study on 2009. The uncertainty presented in these figures is less than those shown in field/block scale data, since it only carries the uncertainty in Neutron Probe calibration curve.

Leaching (L):

The amount water lost through leaching can be calculated using the water balance equation (**Eq. 2**), since all other components are known.

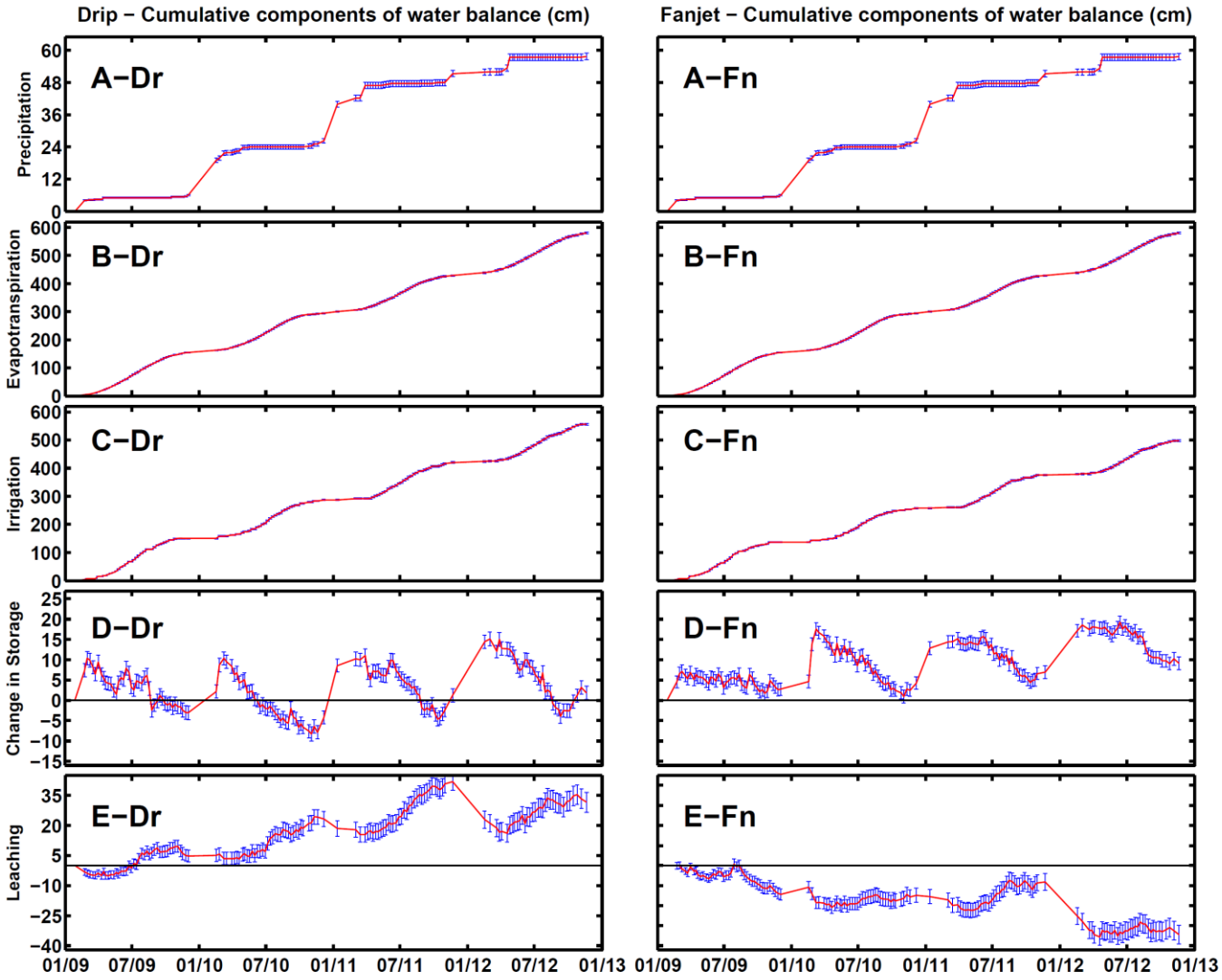

Figure 15. Cumulative amount of (A) precipitation, (B) evapotranspiration, (C) applied irrigation water, (D) change in soil water storage, and (D) leaching in both drip (left) and fanjet (right) trees for four consecutive of years of 2009 - 2013. Average values are presented by the thick red lines, whereas the spatial variations are presented by the error bars, defined by standard deviations.

Field Scale:

Figure 13 E (Fi, Dr, and Fn) presents the calculated cumulative leaching for four consecutive years of the 2009 – 2013 for field, drip block, and fanjet block, respectively. With prior knowledge that the orchard was irrigated based on the ET and depletion of soil water storage, the field average leaching plot confirms a well managed irrigation scheduling with minimum average leaching (almost zero). The uncertainty shown in these figures are mainly introduced by the uncertainty associated with applied irrigation water. It is also shown in the **Figure 14** that locations with high leaching (color bar) correspond to the location with high amount of applied water (size of the circle). A summary of the water balance components is presented in **Table 2**. The applied water in drip block was higher than ET-P (IW > ET-P), while it was smaller for the fanjet field block, resulting in estimated leaching values of 7 cm for the drip block, and estimated upward flow of about - 10 cm into the root zone for the fanjet block. We

note here that all of the calculations were made with the assumption of uniform evapotranspiration (ET) across the orchard. It is known that plants adjust their water demand based on water availability, suggesting that trees with higher applied water transpire higher than the field average ET, and vice versa.

Tree Scale:

Figure 15 E (Dr and Fn) show the cumulative leaching for four consecutive years during the 2009 – 2013 monitoring period for the drip and fanjet tree plots, respectively. As was already discussed, the variation in calculated leaching is mainly derived by differences in applied water since both ET and P are assumed uniform across the orchard, and the annual changes in soil water storage is usually small. The applied irrigation water in drip tree was about 60 cm higher than the fanjet, resulting in a difference of 66 cm in leaching between the drip and fanjet tree plots. The higher value in leaching difference is related to difference in change in soil water storage (1.8 cm for drip vs. 9.1 cm for fanjet).

Table 2. A summary of the water balance components for field, irrigation block, and tree scale for the 2009 - 2013 monitoring period.

	P (cm)	ET (cm)	IW (cm)	ΔS (cm)	L (cm)
Field	57.7 (±1.2)	580 (±3)	522.4 (±19)	1.3 (±5)	-1.3 (±19.7)
Drip block			529.7 (±19.8)	0.1 (±5)	7.1 (±19.5)
Fanjet block			515.1 (±14.8)	2.5 (±4.7)	-9.7 (±16)
Drip tree			555.8 (±3.2)	1.8 (±1.6)	32 (±4.9)
Fanjet tree			497.2 (±2.9)	9.1 (±1.6)	-34.4 (±4.7)

Darcy equation

Leaching rates were computed from the Darcy Eq. [1], considering the uncertainty in (a) soil water matric potential measurements, (b) unsaturated hydraulic conductivity curves, and (c) soil texture of the soil layers at the deep tensiometer locations. Therefore, rather than calculating single leaching rate values, we computed leaching rate uncertainty in addition. However, since the tensiometers were installed in the spring of 2012, we only report values starting May, 2012. The deep soil profile was very dry and as a result the soil matric potential was out of the tensiometery range. We therefore stopped maintaining the deep tensiometers at the end of summer 2013 since the soil profile stayed dry due to the extreme drought condition with almost no meaningful precipitation followed by ~50% reduction in applied water in 2014.

Figures 16 A (Dr and Fn) present the average and standard deviation of matric potential values measured at the 200 and 220 cm soil depths for the drip and fanjet trees, respectively. As a result of increasing root water uptake and crop transpiration from spring to summer, the matric potential of the soil layer below the root zone gradually decreases (more negative) for both trees, but does not increase during the winter due to very low winter rainfall. It is shown that the deep soil matric potential slightly increased over the 2012 irrigation season, but not enough to have meaningful effect on soil leaching. We note that the matric potential values of the drip site are much larger (less negative) than for the fanjet site, because of either the clay layer presence at the tensiometer depth or greater amount of applied irrigation water

discussed in previous section, or both. Moreover, the drier soil at the fanjet site is caused by reduced hydraulic conductivity of the clay layer above the 120 cm soil depth. The much larger uncertainty of the matric head values at the fanjet location is likely caused by the non-uniformity of the water application and reduced lateral spreading above the deep soil layers because of the lower water content at this site (panel B), as opposed to the drip site as caused by higher IW values.

From the measured matric head values at the 200 and 220 cm soil depths, the total head gradient with corresponding spatial variations (standard deviation values) are plotted in **Figure 16 B (Dr and Fn)**. Typically, average total head gradients in fanjet site vary between 2 and 4, indicating downward soil water flow, but gradually decreasing through the summer and fall. However, the tensiometer usually starts to drain at suction of about -700 cm, which would correspond (accounting for tensiometer length ~ 200 cm in our case) to the soil matric potential of -500 cm. Therefore, the gradient obtained at soil matric potential of about -500 or more negative can be over- or under-estimated. The same trend is shown for the drip. Variations are typically large, and are caused by uncertainty in tensiometer readings and soil heterogeneity.

In order to compute the leaching rate at the 200-220 cm soil depth, we need to substitute the unsaturated hydraulic conductivity value of this layer in Eq. [1], which is dependent on soil texture and soil water matric potential at the tensiometer locations. However, because of the large variations in both matric potential and soil texture, we present the range in unsaturated hydraulic conductivity (**Figure 16 C**) as determined from the uncertainty ranges of matric potential (**Figure 16 A**) and unsaturated hydraulic conductivity curves (**Figure 8**). The latter is controlled by soil texture, but is partly unknown because of the apparent high spatial variability of soil texture and soil layering. Therefore, for each tree we calculated the unsaturated hydraulic conductivity of six soil cores collected from two depths of 190 and 210 cm, each with three replications. The unsaturated hydraulic conductivity can varies in order of magnitudes thereby playing as dominant factor in calculating the leaching by Darcy equation. Despite the lower matric potential (less negative) in drip compare to fanjet, the average and range of corresponding hydraulic conductivity are the same (gray horizontal bar in **Figure 8**) as the soil cores from fanjet represent a finer textured soil than those in drip. However, the variation in matric potential for the fanjet is large thereby resulting larger variation in hydraulic conductivity in fanjet compare to drip. The final estimated leaching rate values are presented in **Figure 16 D**, with mean leaching rate values ranging between 0-0.25 (±0.26) cm/day for drip and 0-0.15 (±0.35) cm/day for the fanjet.

In addition to computing leaching rates from the measured unsaturated hydraulic conductivity curves, we include in **Figure 16 F**, the predicted hydraulic conductivity curves and associate uncertainty, using the Neuro Multistep results of **Figure 9**. As the results indicate, the predicted hydraulic conductivities (panels **E**) are close to the measured values for drip. However, the majority of predicted hydraulic conductivities in fanjet falls into the coarse textured soil category resulting very low conductivity at range of matric potential measured in fanjet. **Figure 16 F** show the leaching rates calculated using the hydraulic conductivities estimated by the neural network model.

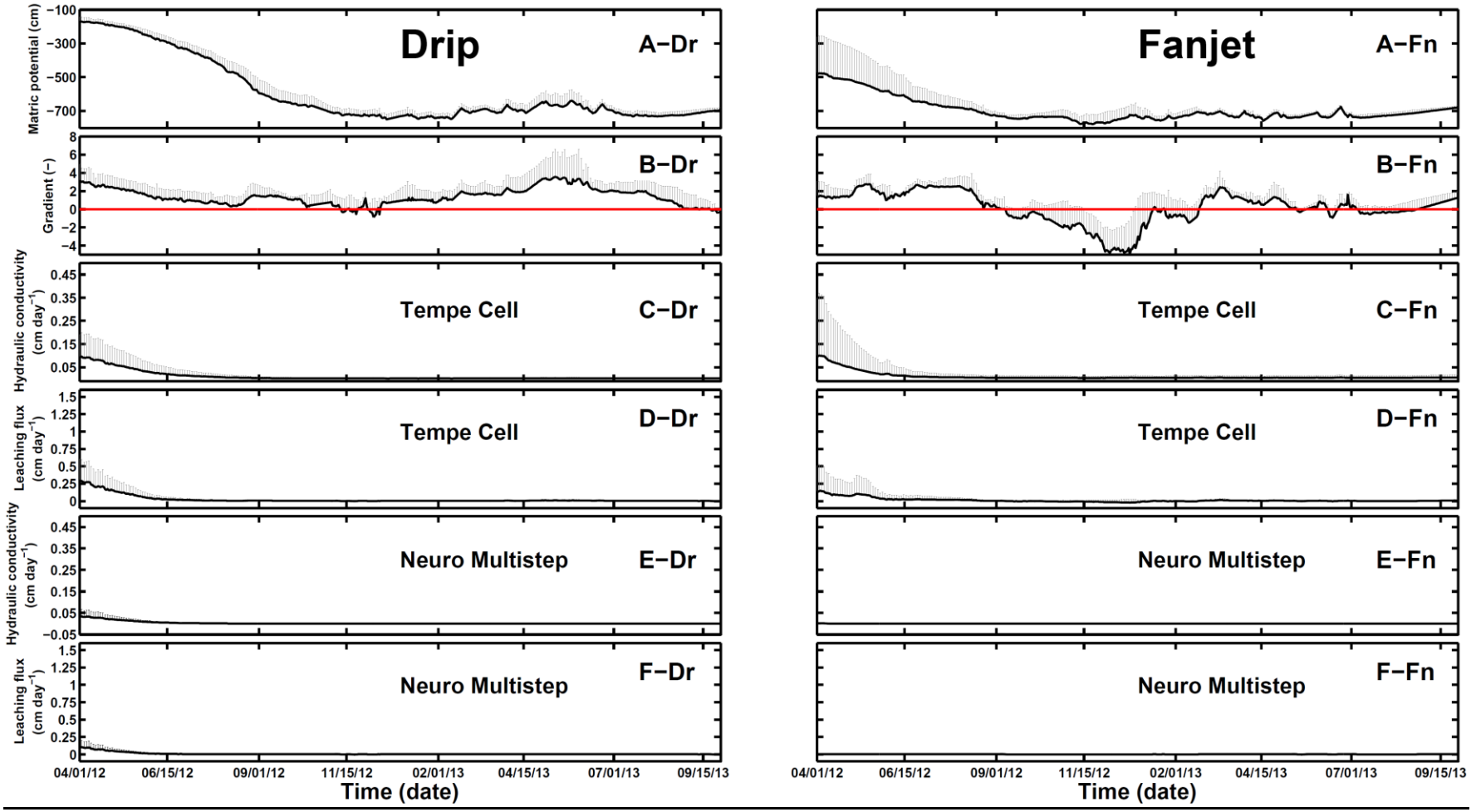

Figure 16. Spatial and temporal variations of (A) matric potential at the 200 and 220 cm soil depth, (B) total head gradient, (C and E) unsaturated hydraulic conductivity for multistep and Neuro Multistep methods, respectively, and (D and F) leaching rate for multistep and Neuro Multistep methods, respectively, as measured for 4 locations (**Figure 1**), starting April 1, 2012 through Sep 30, 2013. Average values are presented by the thick black lines, whereas the spatial variations are presented by the error bars, defined by standard deviations (error bars).

Comparison of leaching between water balance and Darcy equation approaches
Table 3 shows a comparison between the cumulative leaching estimated using the water balance and the Darcy equation approach, using both measured (Multi-step) and predicted Neuro Multi-step)unsaturated hydraulic conductivity curves. We note that the estimated uncertainty is significantly larger for the Darcy calculations, but in general the total cumulative L values are reasonably close between the two methods.

Table 3. Comparison of L and uncertainty range from water balance and Darcy equation approaches.

		Water balance	Darcy-Multistep K(h)	Darcy-Neuro Multistep K(h)
Leaching (cm)	Drip	15.05 (±2.61)	11.6 (±13.6)	3.7 (±3.2)
	Fanjet	-2.1 (±2.41)	6.2 (±15.85)	0.07 (±0.08)

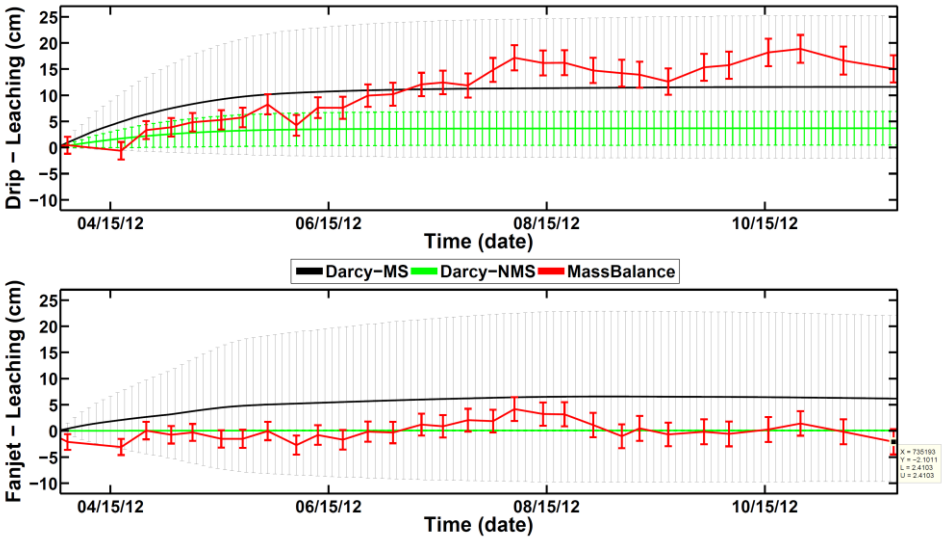

Figure 17. Comparison of leaching and the associated uncertainty range obtained from three different approaches of a) water balance (Red line), b) Darcy equation with measured soil hydraulic properties with combination of constant head and tempe cell (black line), and c) Darcy equation with predicated soil hydraulic properties using NeuroMultistep model (green line).

Figure 17 presents the calculated cumulative leaching using the above mentioned three approaches. The large uncertainty comes from the heterogeneity in soil properties and the corresponding high uncertainty of the soil hydraulic conductivity of the layer below the root zone. Evaluating the uncertainty range presented for drip and fanjet, one could conclude that the main uncertainty come from unsaturated conductivity, especially in the wet end, because L values tend to be near zero in the dry water content range. The uncertainty presented for the mass balance approach is small, because we used a uniform ET along with a small uncertainty for both locations. However, additional uncertainty of leaching rates from the mass balance

approach is caused by unknown spatial variations of local ET and P across the field. We propose that inverse modeling, using HYDRUS and in-situ soil moisture and water potential data will provide a better and more certain approach for estimation of soil hydraulic properties in the future.

Preliminary results of modeling approach to estimate the hydraulic conductivity and leaching.

As was suggested in section (refer to Comparison of leaching between water balance and Darcy equation approaches section) we implemented inverse modeling approach to estimate the soil hydraulic properties which will be used to simulate the leaching of water and ultimately nutrient (nitrate) below the root zone. **Figure 18** shows the comparison between the set of six original soil hydraulic properties and the two effective soil hydraulic properties, in which the later is obtained using inverse modeling. The optimized hydraulic properties significantly differ from each other but remain within the area delimited by the set of original soil types.

Figure 19 shows the observed and simulated soil water storage (top plot), soil matric potential (middle plot), and leaching (bottom plot) below the depth of 210 cm. It is demonstrated that the estimation of soil water leaching can be facilitated by using limited soil water status observations (soil water content at regular depth intervals and soil matric potential at two locations at the bottom of the soil profile) to obtain optimized effective soil hydraulic properties and further quantify leaching using HYDRUS-2D to model the soil water flow within and below the root zone.

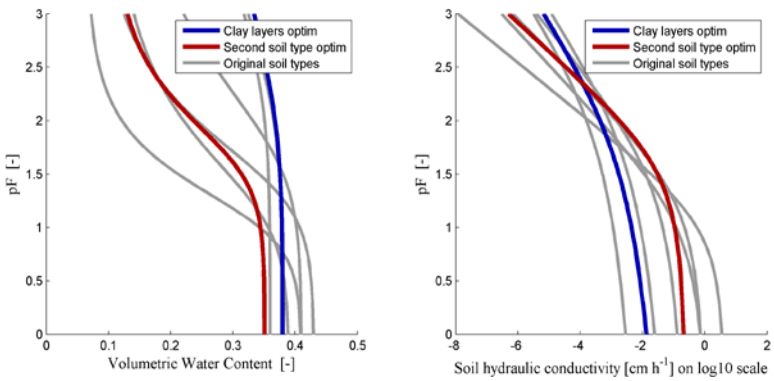

Figure 18. Soil water retention curves (left) and soil hydraulic conductivity curves (right) of the six soil hydraulic types (gray curves) with the optimized clay layers (blue solid lines) and complementary second layer (red solid lines).

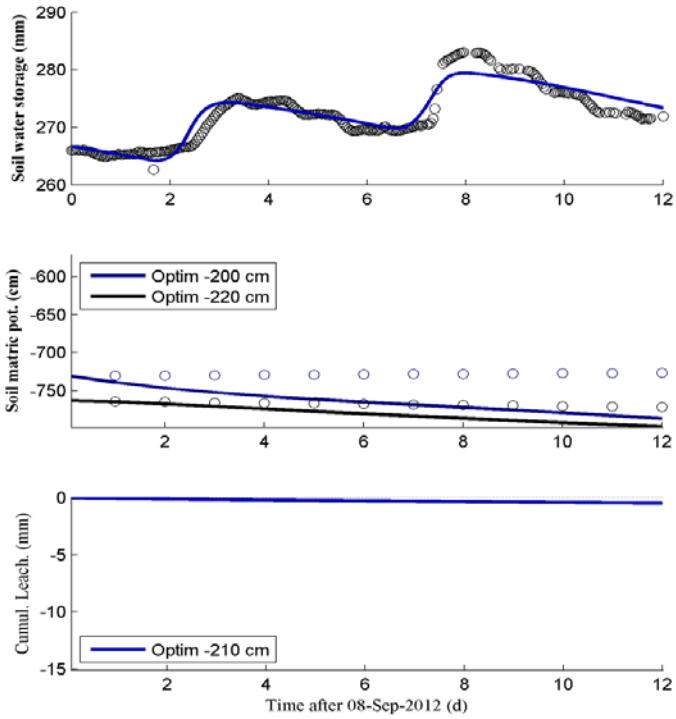

Figure 19. Observed (circle), and simulated (line) soil water storage (top plot), soil matric potential (middle plot), and leaching (bottom plot) below the root zone.

Soil electrical conductivity and nitrate concentration measurements

Figure 20 shows the temporal variations of soil electrical conductivity (EC) at different depths in both fanjet and drip sites, as determined by Blake Sanden. These soil salinity data confirm our hypothesis that the leaching rates are controlled mainly by the amount of applied irrigation water and also by the most shallow clay layer within the soil profile (as represented by the gray bands in **Figure 20**).The lower leaching rates cause higher soil salinity in the soil profile of the fanjet site.

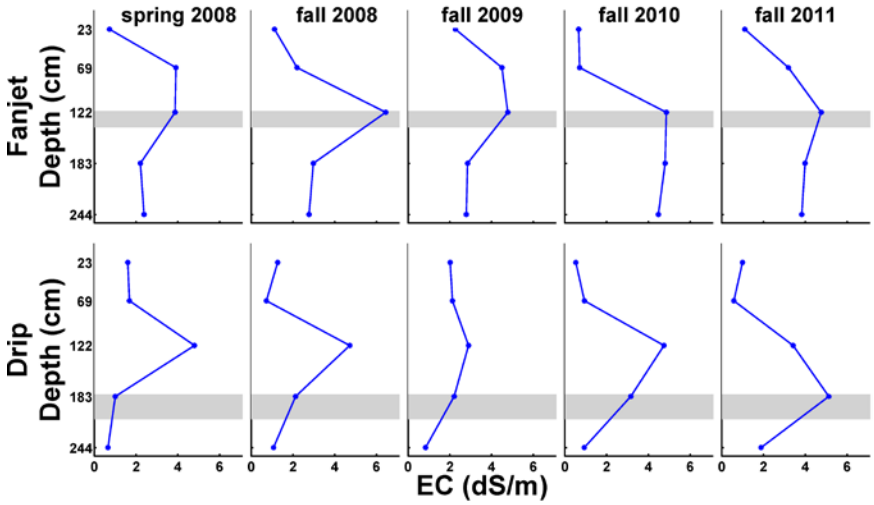

Figure 20. Temporal variations of soil electrical conductivity (EC) at different depth in both fanjet and drip sites. The horizontal gray bar represents the clay layer. Data provided by Blake Sanden.

Figures 21 and **22** show the temporal variations of soil nitrate concentration at different depths (each row of subplots represents different depth) for a series of days after each fertigation. The soil nitrate mass is at minimum before fertigation, then increases to a maximum immediately after fertigation and gradually decreases as nutrient is taken up by tree root uptake or leaches downwards. Much of the lack of soil nitrate solution data are attributed to later installation of solution samplers at the larger soil depths, and inability to extract soil solution because of too dry soil conditions (especially for fan jet site). Spatial variations in nitrate concentration are caused by non-uniform water and associated nutrient applications, non-uniform root nutrient uptake, and spatial variations in soil water content.

To date the nitrate measurement show that there is no general change in soil nitrate storage between fertigations, indicating that all applied nitrate is either taken up or lost by leaching/denitrification. Although not shown here, nitrate losses by denitrification are general very low and are less than one percent of the total applied nitrate (Dave Smart lab). With leaching rates determined to be near zero for most of the growing season, we can therefore assume that most of the applied nitrate is taken up by the almond crop, except for the early spring period when the soil is wet and leaching occurs. In the coming year, we will combine the soil nitrate data with applied nitrate and biomass nitrate information, and complete a total nitrate mass balance for both sites. Tentatively though our data suggest that nitrate losses are likely to occur only in the winter and spring period with relatively high rainfall, when the soil is wet and root water uptake rates are relatively low.

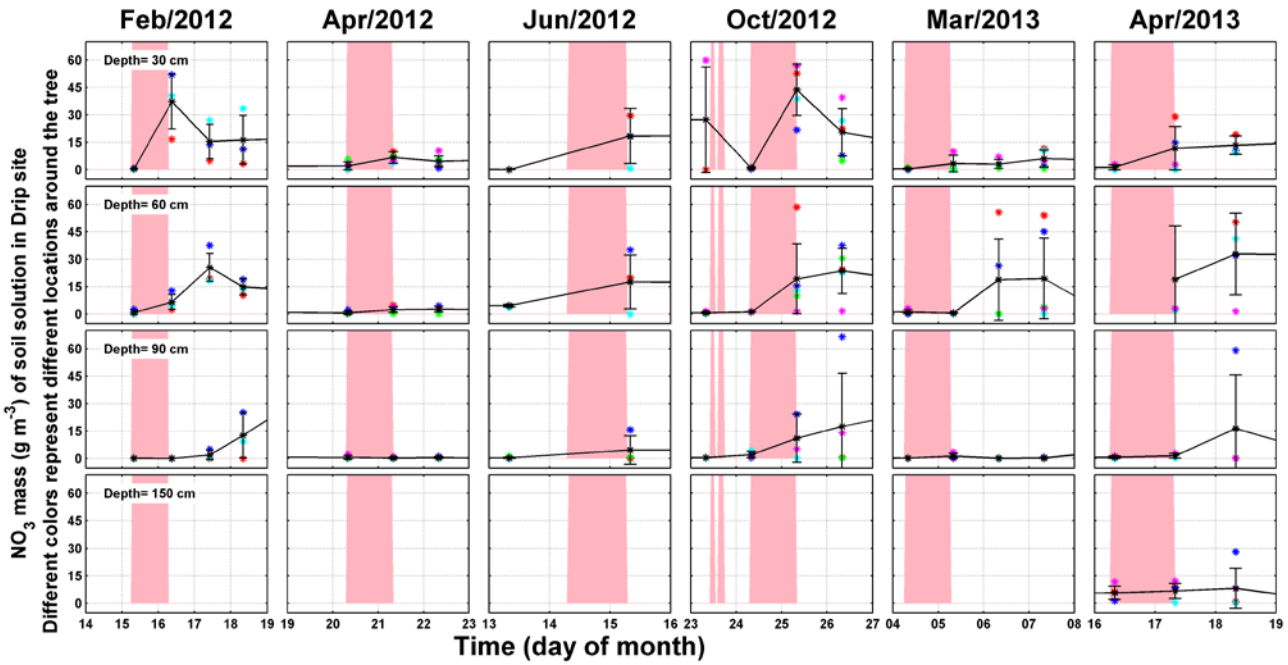

Figure 21. Temporal variations of soil nitrate mass (g m^{-3}) at different depths in **drip** site after each fertigation. Different colored points represent different location around the tree. The pink bar shows the period of fertigation event.

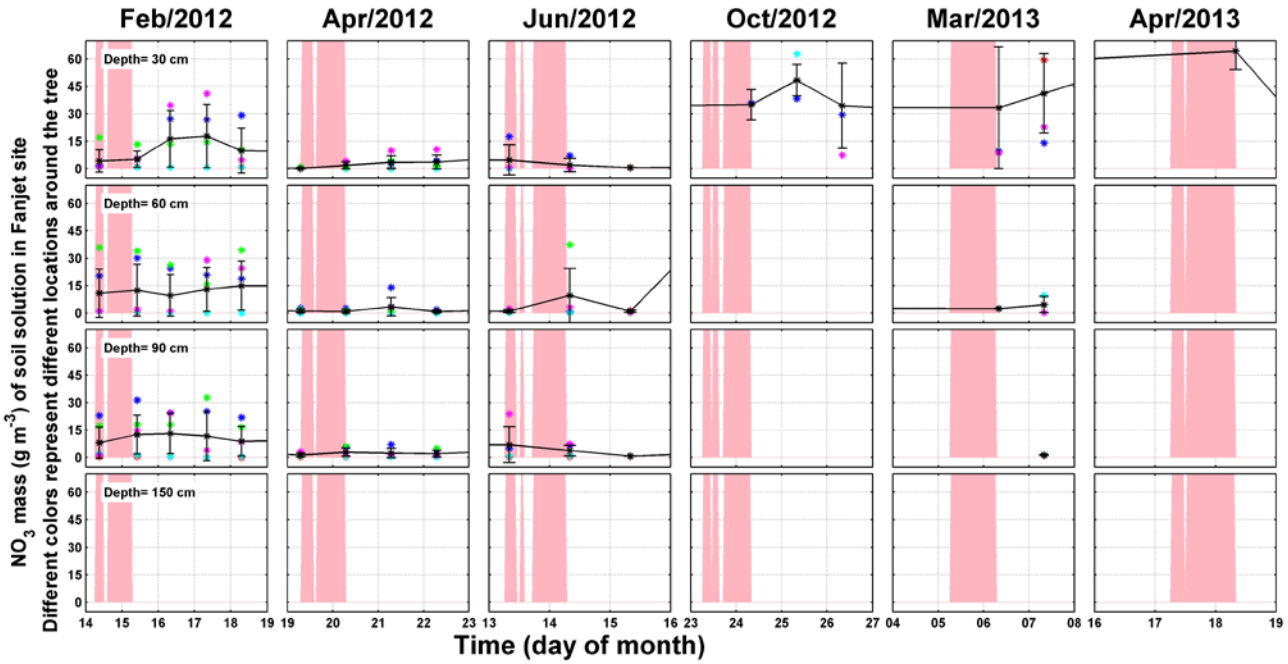

Figure 22. Temporal variations of soil nitrate mass (g m^{-3}) at different depths in **fanjet** site after each fertigation. Different colored points represent different location around the tree.

Research Effort Recent Publications:

Kandelous, M.M., Moradi, A. B., Couvreur, V., Baram, S., Hopmans, J. W. 2014. Monitoring and modeling of nitrate leaching in micro irrigation across a wide range of California crops and soils. Soil Science Society of America, Long Beach, CA.

Kandelous, M.M., Sanden, B., Hopmans, J.W., 2013. A Unified Experimental Approach for Estimation of Root Zone Leaching of Applied Irrigation Water and Fertilizers. Soil Science Society of America, Tampa, FL.

Kandelous, M.M., Olivos, A., Sanden, B., Brown, P., Hopmans, J.W., 2013. Optimization of Water Use and Nitrate Use for Almonds under Micro-Irrigation. Almond Board of California annual Meeting. Sacramento, CA.

Kandelous, M.M., Moradi, A.B., Brown, P., Hopmans, J.W., 2013. Monitoring of water and nitrate leaching in an almond orchard, American Geophysical Union Fall Meeting, San Francisco, CA.

Hopmans J.W., and Kandelous, M. M. 2013. How does Nitrogen move in the soil, and what are the factos that influence its movement. Citrograph, May/June 2013, pages 22-28.

Kandelous, M.M., Moradi, A.B., Hopmans, J.W., Burger, M., 2012. Coupled experimental-modeling approach for estimation of root zone leaching of applied irrigation water and fertilizers, AGU Fall Meeting. AGU, San Francisco.

Kandelous, M.M, A. Olivos, P. Brown, and J.W. Hopmans, 2012. Optimization of water use and nitrate use for almonds under micro-irrigation. Almond Industry Conference, Sacramento, CA.

Kandelous M.M., T. Kamai, J.A. Vrugt, J. Simunek, B.R. Hanson, and J.W. Hopmans. 2012. Evaluation of subsurface drip irrigation design and management parameters for alfalfa. Agric. Water Management. Doi:10.1016/j.agwat.2012.02.009.

Kandelous, M.M, A. Olivos, P. Brown, and J.W. Hopmans, 2011. Optimization of water use and nitrate use for almonds under micro-irrigation. Almond Industry Conference, Modesto, CA.

Hopmans, J.W., M.M. Kandelous, A. Olivos, B.R. Hanson and P. Brown. 2010. Optimization of water use and nitrate use for almonds under micro-irrigation. Almond Industry Conference, Modesto, CA.

Kandelous, M.M, T. Kamai, J.A. Vrugt, J. Simunek, B.R. Hanson and J.W. Hopmans. 2010. An optimization model to design and manage subsurface drip irrigation system for alfalfa. AGU Fall meeting, San Francisco, CA.